PCCP

Towards Bridging the Structure Gap in Heterogeneous Catalysis: The Impact of Defects in Dissociative Chemisorption of Methane on Ir Surfaces

Journal:	*Physical Chemistry Chemical Physics*
Manuscript ID	CP-ART-12-2020-006535.R1
Article Type:	Paper
Date Submitted by the Author:	22-Jan-2021
Complete List of Authors:	Zhou, Xueyao; University of Science and Technology of China Zhang, Yaolong; University of Science and Technology of China Guo, Hua; University of New Mexico Jiang, Bin; University of Science and Technology of China

ARTICLE

Towards Bridging the Structure Gap in Heterogeneous Catalysis: The Impact of Defects in Dissociative Chemisorption of Methane on Ir Surfaces

Received 00th January 20xx,
Accepted 00th January 20xx

DOI: 10.1039/x0xx00000x

Xueyao Zhou,[a,b] Yaolong Zhang,[a] Hua Guo,[b,*] and Bin Jiang [a,*]

A quantitative understanding of the role played by defect sites in heterogeneous catalysis is of great importance in designing new and more effective catalysts. In this work, we report a detailed dynamic study of a key step in methane steam reforming under experimentally relevant conditions on a new high-dimensional potential energy surface determined from first principles data with the aid of machine learning, with which the interaction of CH_4 on the flat Ir(111) and stepped Ir(332) surfaces are both described. In particular, we argue based on our simulations that the experimentally observed "negatively activated" dissociative chemisorption of methane on Ir surfaces could be due to a combined effect of defects and high substrate temperature, which lowers the reaction barrier relative to that on terraces. Furthermore, a model based on dynamic information of trapping and reaction channels is proposed, which allows a quantitative prediction of the initial sticking probability for different defect densities, thus helping to close the so-called structure gap in heterogeneous catalysis.

Introduction

Chemical reactions occurring at the gas-surface interface are essential to many important processes, such as heterogeneous catalysis, corrosion prevention, and crystal growth. These processes often involve multiple elementary steps that can take place at different active sites,[1] so a better understanding at the atomistic level is highly desirable. In particular, under realistic conditions, catalyst surfaces often consist of not only atomically flat terraces, but also under-coordinated defects, such as steps and kinks. In many cases, these defects represent dominant active sites for catalysis, offering lower activation barriers than terraces.[2-4] These differing characteristics present an ideal proving ground for studying site specificity under well-defined conditions, using dynamic methods such as molecular beam scattering. As a result, there has recently been an increasing interest in studying surface reaction dynamics on stepped surfaces[5-11] and exquisitely-crafted curved surfaces containing a varying step density,[12, 13] which help to reveal the site sensitivity of surface reactions.[6, 9, 14] Such studies are necessary to bridge the "structure gap" between the well-ordered metal facets studied in surface science and defect laden real catalysts.[15]

Indeed, even a well-prepared single crystal surface is not completely defect-free, typically with a step density of about a few thousandths. Even such a low defect density could potentially affect surface reactivity and dynamics in a significant way. At low incident energies (E_i), for example, atomic steps have long been argued to play a controlling role in dissociative adsorption of hydrogen on platinum,[4] even on a near-perfect Pt(111) surface with ~0.1% step density.[16, 17] Using a curved platinum surface, Juurlink and co-workers have recently revealed that the initial dissociative sticking probability (S_0) of H_2 on Pt is step-type dependent and varies linearly with step density, which was interpreted as a linear combination of site-specific reactivities.[13] Another example is CO oxidation over platinum surfaces, in which the reactive site influences product energy disposal. On a Pt(111) surface with a step density of ~0.25%, the CO_2 products are observed with a bimodal velocity distribution, corresponding to a thermal channel taking place at the more active step sites and a hyperthermal one at the more abundant terrace sites, respectively.[14] These two distinct mechanisms have been recently confirmed by theory, which were ascribed to the post-transition state dynamics and the involvement of a chemisorbed CO_2 species in the step edges.[18]

The focus of the present work is on another prototypical system that may have an exquisite involvement of steps, namely the dissociative chemisorption of CH_4 on iridium surfaces. As the initial and rate-limiting step in the steam reforming of natural gas, the dissociative chemisorption of methane on transition metals has been extensively investigated.[19-29] Most experimental data indicate that this reaction is a direct and strongly activated process at high incidence energies, where the initial sticking probability (S_0) increases monotonically with increasing E_i. However, at low collision energies (*e.g.*, E_i < 0.10 eV or so) and high surface temperature (e.g. T_s > 800 K), an indirect and "negatively activated" regime was observed on Ir(110) and Ir(111) surfaces, where S_0 decreases with increasing E_i.[30-32] Furthermore, Utz and co-workers found that this mechanism persists for vibrationally excited methane.[33] (Similar "negatively activated" regimes have also been reported for methane dissociation on the Pt(110)-2×1 surface.[34, 35]) This behavior is of great importance not only for fundamental understanding of surface reaction dynamics, but also for practical applications because steam reforming typically operates at 700-1000 °C, which correspond roughly to a low translational energy of 0.1 eV and a sizable population of vibrationally hot molecules. This "negatively activated" behavior is believed to be a signature of an indirect precursor-mediated (or trapping-mediated) mechanism,[30, 31] in which the

[a] Hefei National Laboratory for Physical Science at the Microscale, Department of Chemical Physics, University of Science and Technology of China, Hefei, Anhui 230026, China. Email: bjiangch@ustc.edu.cn
[b] Department of Chemistry and Chemical Biology, University of New Mexico, Albuquerque, New Mexico 87131, USA. Email: hguo@unm.edu
Electronic Supplementary Information (ESI) available: [details of any supplementary information available should be included here]. See DOI: 10.1039/x0xx00000x

impinging molecule loses sufficient kinetic energy to be trapped on the surface and the trapped "precursor" molecules undergo diffusion on the surface and may react when an active site is encountered. Since trapping only occurs at low energies, this mechanism becomes less important with increasing E_i.

The aforementioned picture of the "precursor-mediated" mechanism has attracted much recent theoretical attention. The earlier molecular dynamics (MD) work of Sitz and Mullins using an empirical interaction potential predicted extensive trapping of CH_4 at low incidence energies and diffusion on Ir(111).[36] The dissociation of methane on Ir(111) was studied by Henkelman and Jónsson, who showed using density functional theory (DFT) that the barrier can be lowered by the puckering of the underlying Ir atom,[37] a common feature in methane dissociation on transition metal surfaces.[26] More recently, Busnengo and co-workers pointed out based on static DFT calculations that high surface temperatures could lead to large fluctuation of surface Ir atoms and hence lower the reaction barrier.[38] In addition, the energy barrier in monoatomic steps of an non-perfect Ir(111) surface is significantly smaller than that on a perfect terrace of Ir(111).[38] Indeed, recent MD simulations from the same group[39] based on a DFT parameterized reactive force field (RFF) for CH_4+Ir(111) provided further theoretical evidence that trapped CH_4 molecules can undergo extensive diffusion and eventually dissociate at thermally fluctuated surface sites with sufficiently low barriers generated by heavily-distorted surface structures at high surface temperatures. Subsequent work by Jackson[40] treated the indirect reactivity as the relative ratio of chemisorption and desorption rates of physisorbed molecules determined by transition-state theory, providing a kinetic perspective of the process in thermal equilibrium.

Despite these advances, our knowledge of the complex interplay of scattering, trapping, diffusion, and dissociation in this prototypical system is still far from complete, particularly concerning the role played by surface defects. Jackson recently estimated that even at the step density of 0.5%, the defects on Ir surfaces are expected to significantly affect the results at low incidence energies.[40] In a recent study, we have investigated the role played by defects in dissociative chemisorption of CH_4, using a stepped Ir(332) surface as a model.[41] Our DFT calculations confirmed that the barrier for methane dissociation is much lower at step sites than that on terraces and the barrier is strongly modulated by surface temperature, much the same way as in the case of Ir(111). Furthermore, significant trapping and diffusion have been observed in *Ab Initio* Molecular Dynamics (AIMD) simulations. However, these AIMD calculations are extremely expensive and can only be carried in small numbers and for short time durations. In this work, we present an extensive MD study on the tapping, diffusion, and dissociation of both the ground state and vibrationally excited CH_4 on Ir surfaces using a new unified high-dimensional potential energy surface (PES) that includes the motion of both CH_4 and surface Ir atoms. This PES, which was constructed with a machine learning algorithm based on a large number of DFT energies and gradients, describes the interaction of CH_4 with both the flat Ir(111) and stepped Ir(332) surfaces, thus bypassing the expensive on-the-fly DFT calculations in trajectory calculations. These first-principles based calculations provide important insights that can be used to test fundamental assumptions in more coarse-grained models. Furthermore, we propose a model that is capable of predicting reactivity for Ir surfaces that have an arbitrary density of step sites over a large energy range. Through detailed investigations of this exemplary system, we hope to advance our knowledge on quantitative characterization of heterogeneous catalysis on imperfect catalyst surfaces.

Computational Details

Static DFT calculations and AIMD simulations have been performed with the Vienna *Ab initio* Simulation Package (VASP)[42, 43] using the optPBE-vdW functional,[44] which was shown to provide a balanced description of this system, especially for the physisorption well.[41] The 322 facet consists of periodically one atomic row of steps every six rows, which was modeled by a 10 layer slab in a 3×1 supercell with the size of (12.918 Å × 8.263 Å), where the top six layers were allowed to move. To keep the cell size and the number of Ir atoms in the cell similar to Ir(332), a 3×5 supercell (13.771 Å × 8.263 Å) with a 4-layer slab was used for Ir(111) with the top two layers moveable, which was slightly different from that used in Ref. 41.

To enable the extensive dynamical calculations, a high-dimensional and high-fidelity PES for methane dissociation on Ir surfaces was constructed based on previous AIMD and DFT calculations[41] using a machine learning based, so-called piecewise embedded atomic neural network (PEANN) method.[45, 46] Such machine learning approaches have been successfully applied in several molecule-surface systems with numerical savings on the order of 10^5.[47] An important character of this new PEANN PES is that it describes methane interacting with both the (111) and (332) facets of Ir, even at high temperatures. Quasi-classical trajectory (QCT) calculations were performed on this PES for CH_4 in laser-off conditions and with antisymmetric stretching mode excited ($1\nu_3$) dissociative adsorption on Ir(111) and Ir(332) surfaces, at a wide range of incident energy from 0.01 to 0.5 eV mimicking experimental conditions at T_s = 1000 K.[33] A large number of trajectories were run to reach reasonable statistical errors, especially at low energies. More details on the DFT and QCT calculations, data sampling and PEANN training are given in the Supporting Information (SI).

For both terrace and defect sites, it is straightforward to calculate the initial dissociative sticking probability (S_0) by QCT at high incident energies where the dissociative adsorption takes place directly upon collision. At low incident energies, however, the impinging methane molecule may lose sufficient energy and be trapped in a physisorption state forming a "precursor". As shown in a recent MD study of Moiraghi *et al.*, the energy of the impinging CH_4 along the Z direction is rapidly dissipated within 2.5 ps once it is trapped on Ir(111), but the momentum parallel to the surface is not equilibrated even up to 45 ps.[39] It is therefore very difficult to determine the indirect dissociative sticking probability from dynamical calculations

because of the long trapping lifetime. In what follows, we describe a model that is capable of accounting for the impact of the defect sites in methane dissociation.

First, we estimate the probability of a trapped precursor to find a defect site on a surface on which the average distance between defect sites is given by L_d. Following Comsa and co-workers,[16] this diffusion probability can be approximated as follows,

$$P_{\text{diff}} = \frac{v\tau}{L_d}\left(1 - e^{-\frac{L_d}{v\tau}}\right), \quad (1)$$

where the trapped molecule is assumed to have a residence time (τ) and moves with a lateral velocity (v) on the surface. Provided that the trapping probability of the incident molecule into the physisorption well (P_{trap}) and the dissociation probability at a defect site (P_{diss}) are both known, the indirect dissociative sticking probability at the defect site can be estimated as,

$$S_{0,\text{defect}}^{\text{indirect}} = P_{\text{trap}} P_{\text{diff}} P_{\text{diss}}, \quad (2)$$

In the case of CH_4 dissociation on a real iridium surface, we can envision the surface contains both terrace and defect sites. The total S_0 on such an imperfect surface is thus the sum of direct and indirect contributions at defect sites, as well as S_0 at terrace sites,

$$S_0 = S_{0,\text{defect}}^{\text{indirect}} + \theta_d \cdot S_{0,\text{defect}}^{\text{direct}} + (1-\theta_d) S_{0,\text{terrace}}, \quad (3)$$

where θ_d is the defect density conventionally defined as the fraction of defect sites in total sites on the surface, which is a dimensionless quantity between 0 and 1.

To simplify our discussion, the defect is assumed to be a step site in this work. It should be noted that individual contributions to the total S_0 can be estimated by fitting experimental data to approximate functions, as done for H_2 on Pt by Juurlink and coworkers.[6, 48] However, we extract all quantities here from first-principles dynamical calculations. For example, we can find $S_{0,\text{defect}}^{\text{direct}}$ from the direct dissociation of CH_4 at step sites on Ir(332) and $S_{0,\text{terrace}}$ on a clean Ir(111). P_{trap} is the initial trapping probability of the incident molecule entering into the physisorption well (*vide infra*). P_{diss} is simply approximated by $S_{0,\text{defect}}^{\text{direct}}$ at a given kinetic energy ($mv^2/2$), assuming that parallel momentum is equally effective as normal momentum in molecular dissociation at step sites. Although this total energy scaling may not be valid at high energies, it was found to work reasonably well at low energies for trapping-mediated chemisorption where the parallel momentum can be redirected into the normal direction on rougher surfaces like Ir(110),[30] which should also work in our case at step sites in the energy range where the indirect contribution to S_0 is dominant. The average residence time (τ) can be estimated by assuming an exponential decay of trapping probability as a function of time and the lateral velocity (v) is an average over trapped trajectories. L_d is roughly associated with θ_d by $L_d = d_{Ir}\theta_d^{-1}$ where d_{Ir} is the equilibrium Ir-Ir distance on the Ir(111) terrace. It is important to note that these parameters can be obtained for both thermal and nonthermal CH_4 molecules at a specific vibrational state.

With this setup, we can estimate S_0 of CH_4 initiated in any conditions on defected Ir surfaces using this model. At high incident energies, both defect and terrace sites are reactive and the reactivity is typically dominated by the vast number of terrace sites. At low incident energies, however, the defect sites could become dominant if the contributions from terrace sites are turned off due to their higher barriers. This is the case in the current system, where the dissociation barrier at the step is significantly lower than that on terrace. As a result, the indirect contribution to the overall S_0 can be significant at low energies where the trapping probability is large and the residence time is long, even if θ_d is low (or equivalently L_d is large), as we illustrate below.

Results and Discussion

The fitting root-mean-square error (RMSE) of the PEANN PES over the ~15000 data points for the CH_4+Ir system distributed in a wide energy range (up to 9 eV relative to CH_4 plus an equilibrium Ir surface) is 17.6 meV for energy per cell (~0.3 meV/atom) and 58.0 meV/Å for force. More detailed comparisons of stationary point geometries and energetics, as well as substrate atom displacement distributions represented by DFT and PES are provided in the SI. Specifically, the PES reproduces these stationary points for CH_4 physi- and chemisorption on Ir(332) and Ir(111) equally well. For example, the physisorption well depths on the PES are found to be 0.168 and 0.253 eV on the flat Ir(111) and stepped Ir(332) surfaces, respectively, which deviate from the DFT values directly optimized in the slab model by merely 6 meV. The well depth on Ir(111) is in good accord with previous theoretical results, namely ~0.18 eV in Ref. 39 and 0.215 eV of Ref. 40, and the estimated experimental values of ~0.127 eV on Ir(111)[49] and ~0.19 eV on Ir(110).[30] It is emphasized that this physisorption well is properly captured by the optPBE-vdW functional here (see Figure S2), while was adjusted in an empirical way in the RFF based on PBE.[39] The PEANN PES yields a dissociation barrier of 0.684 eV on Ir(111) and of 0.241 eV on Ir(332), respectively, differing from the DFT values by less than 25 meV. Note that these energies are all relative to the reactant energy of a free CH_4 above the surface.

An important feature of methane dissociation on Ir surfaces is that the surface atom displacement has a pronounced effect on the dissociation barrier.[37, 38, 41] This is confirmed in Figure 1, the barrier height is linearly dependent on the vertical shift of the underlying Ir atom from equilibrium on Ir(111) with a slope of $\Delta E_b/\Delta Z_{Ir}$ = -1.38 eV/Å, which reproduces our earlier DFT result[41] (-1.41 eV/Å) well. It is however much smaller than that on RFF based on PBE[50] calculations (roughly -1.7 eV/Å).[39] It is interesting to note that the slope (1.56 eV/Å) in Ref. 40 based on the SRP32-vdW functional[51] is also smaller than the RFF value. On Ir(332), on the other hand, $\Delta E_b/\Delta Z_{Ir}$ is reduced to -0.96 eV/Å, which is again in excellent agreement with the DFT value of -0.94 eV/Å.[41] Detailed comparison can be found in Table S5 of the SI.

In Figure 2, we compare the QCT calculated dissociative sticking probabilities of CH_4 in the laser-off condition and in the $(1\nu_3)$ state on Ir(111) at T_s = 1000 K on the PEANN PES, with available experimental and theoretical data on Ir(111). As expected, most dissociative trajectories occur directly. Our

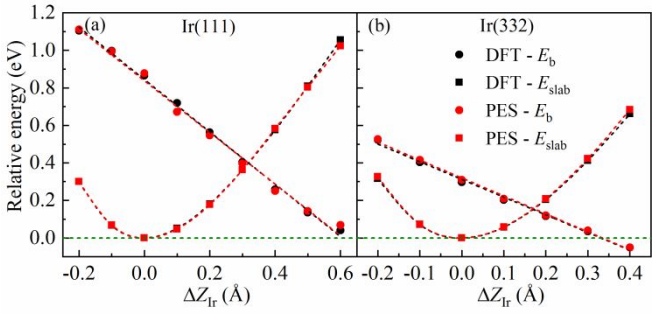

Figure 1. Variation of the dissociation barriers (Eb) and energy cost to distort the surface atom (E_{slab}) as a function of the vertical displacement of the underlying Ir atom (ΔZ_{Ir}) in DFT calculations (black symbols) and on PEANN PES (red symbols) on (a) Ir(111) and (b) stepped Ir(332). E_b is relative to the energy of the equilibrium CH_4 plus the distorted Ir surface.

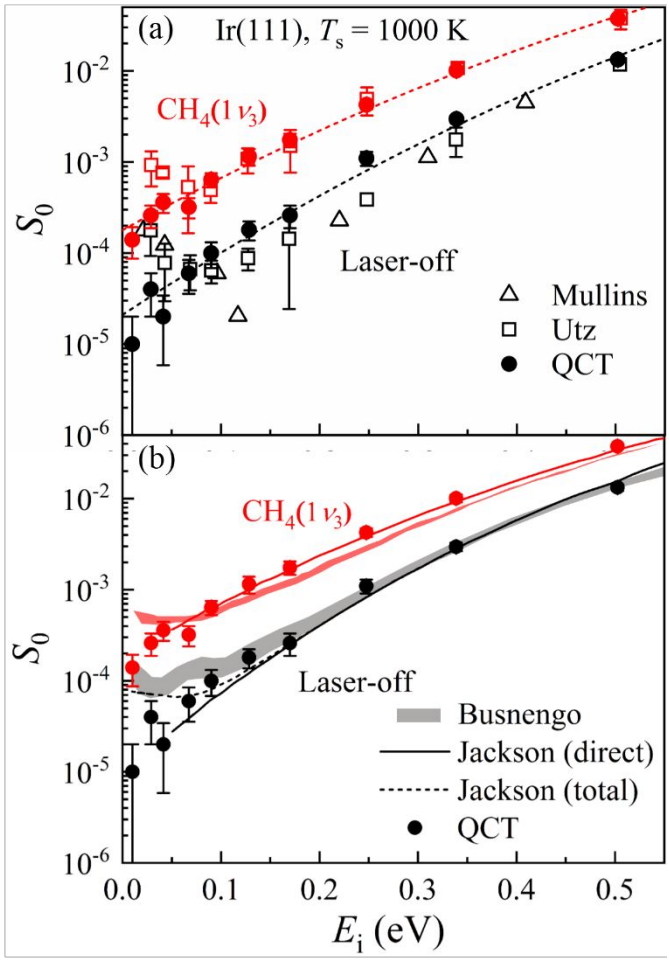

Figure 2. Comparison of S_0 of CH_4 on Ir(111) in laser-off (black) and $CH_4(1\nu_3)$ (red) conditions calculated using the QCT method on PEANN PES (solid circles) and (a) available experimental data (open triangles and squares) extracted from Refs. 31 and 33, and (b) theoretical data from Ref. 39 (shaded areas) and Ref. 40 (solid and dash lines) at T_s = 1000 K. The dash lines in (a) are from the fitting of QCT data using error functions, the total S_0 (black dash line) in (b) is the direct and indirect dissociative sticking probabilities on the perfect Ir(111) surface form Figure 8 in Ref. 40.

results agree quite well with experimental ones in the high-E_i region from 0.1 to 0.5 eV, especially for $CH_4(1\nu_3)$. The calculated vibrational efficacy of $CH_4(1\nu_3)$ relative to translation, which corresponds to the horizontal energy shift between the ground state and $(1\nu_3)$ S_0 curves in Figure 2a divided by the vibrational excitation energy, is 0.32. This compares reasonably well to previous QCT (0.25 in Ref. 39) and approximate quantum model (0.27~0.36 in Ref. 40) predictions, as well as the experimental value (0.43).[33] Although there is inevitable energy randomization between the stretch modes with the similar frequencies in CH_4 $(1\nu_3)$ before reaching the interaction region in QCT calculations (see the harmonic vibrational energy variation as a function of time in Figure S3), this does not weaken the vibrational enhancement of the $1\nu_3$ mode on reactivity. At very low incident energies where the molecule stays very long at the surface, some artificial vibrational energy leakage to the reaction coordinate is possible to increase the S_0. This may contribute to the negative activation in Ref. 39, but certainly not in our work. Since the defect sites and the precursor mechanism have a limited impact on direct dissociation at high incident energies, the good agreement with high energy experimental results suggests that the PES, particularly the dissociation barrier, is accurate.

However, our calculated S_0 curves on Ir(111) monotonically decrease with the decreasing E_i in the low-E_i regime (E_i < 0.1 eV), in disagreement with the observed negatively-activated behavior.[33] Our results are also different from the recent MD results of Busnengo and coworkers based on their PBE-parameterized RFF[39] (see Figure 2b). These authors found a negatively activated region (E_i < ~0.05 eV) in their Ir(111) S_0 curves and attributed it to the larger trapping probability at a lower energy and sufficiently low barrier heights at the surface sites generated by considerable surface atom fluctuations.[39] This discrepancy may be partly due to the fact that the static energy barrier is somewhat lower on their RFF (0.62 eV)[39] than that on our PEANN PES (0.68 eV) based on the optPBE-vdW functional. More importantly, vertical displacements of the underlying surface atom lead to a more dramatic lowering of the dissociation barrier on their RFF than on our PEANN PES, as discussed above. Indeed, the RFF barrier height is lowered to zero by the surface atom displacement of ΔZ_{Ir} = 0.5 Å, which is accessible by thermal fluctuations at T_s = 1000 K (see Figure S4), thus responsible for some dissociation of temporarily trapped molecules.[39] In comparison, the dissociation barrier on our PES remains as high as 0.14 eV at ΔZ_{Ir} = 0.5 Å, so that those trapped molecules have little chance to dissociate at the same surface temperature. This difference indicates that the calculated low-energy S_0 curve is highly sensitive to the PES used in the dynamical calculations and the corresponding functional used in the DFT calculations. The difference with the quantum reaction path Hamiltonian results of Jackson[40] is less clear, as the applied methods involve many respective approximations, which may be roughly ascribed to quantum effects or artefacts of the QCT calculations.

Interestingly, on the stepped Ir(332) surface, our calculated S_0 curves in the low-E_i region are about two orders of magnitude larger than those on Ir(111), as shown in Figure 3a, although the difference diminishes at larger E_i. Importantly, we find a slight decrease of reactivity with increasing E_i in this energy range, an evidence of a precursor-mediated reaction mechanism. The presence of such a channel on Ir(332) rather than on Ir(111) is due apparently to the much lower barriers at steps than that on terraces. Indeed, the static dissociation barrier with a relaxed

surface is merely 0.24 eV at the step edge on Ir(332) with $\Delta E_b/\Delta Z_{Ir}$ = -0.96 eV/Å. The corresponding dissociation barrier almost vanishes at $\Delta Z_{Ir} \approx 0.33$ Å, well accessible by thermal motion at T_s = 1000 K (see Figure 1b). In such a case, trapped CH_4 molecules on terraces may diffuse to a step site with a low or null barrier to react.

Next, we focus on the precursor-mediated mechanism using reactive trajectories for $CH_4(1\nu_3)$. This is because the corresponding statistical errors are much smaller than laser-off

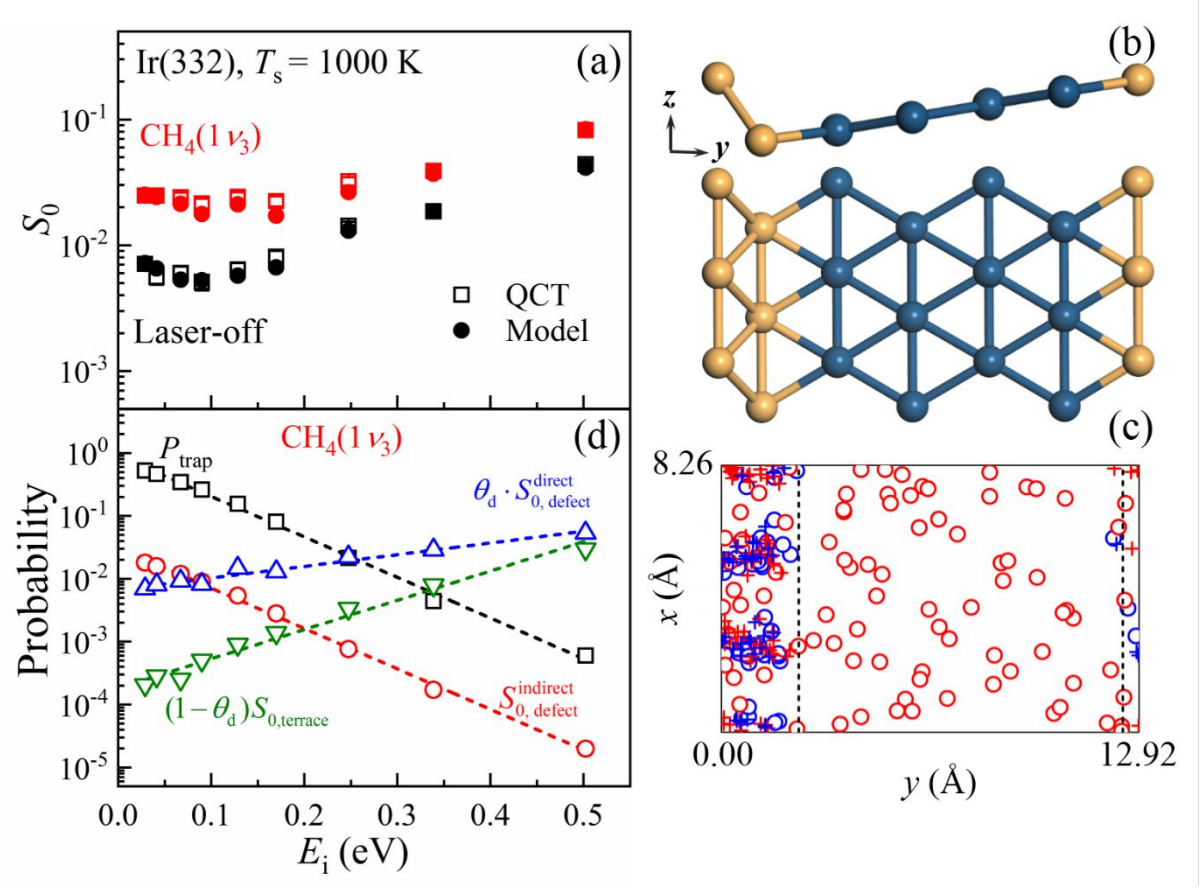

Figure 3. (a) Comparison of S_0 of CH_4 on Ir(332) from QCT calculations (squares) and prediction of the model (circles) for CH_4 initially in laser-off conditions (black) and ($1\nu_3$) state (red), T_s = 1000 K. (b) Side and top views of the Ir(332) surface of a 3 × 1 supercell with the step zone roughly marked in yellow. (c) Scattered distributions of the initial CH_4 centre of mass positions (open circles) and these at the dissociation sites (crosses) of reactive trajectories at E_i = 0.03 eV on the Ir(332) supercell. Direct (indirect) reactive trajectories are labelled with blue (red) circles, corresponding to the impact time shorter (longer) than ~800 fs, or almost equivalently to a single (multiple) bounce(s) of CH_4 on the surface. We define the "dissociation" point when a C-H bond first elongates to 1.60 Å. The dash lines are the dividing surfaces for step and terrace zones used in this work. (d) Initial trapping probability and individual contributions to the total S_0 of $CH_4(1\nu_3)$ predicted by the proposed model, as a function of E_i.

ones, but the physics is essentially similar. Specifically, the two nearby atomic rows at the step edge as marked by in Figure 3b define the step zone on Ir(332) and the remaining area represents the terrace, in accord with the conventionally defined step density,[52, 53] namely $\theta_d = d_{Ir} L_d^{-1}$, where L_d = 12.92 Å being the distance between two nearest step edges in *Y* direction and d_{Ir} = 2.75 Å being the Ir-Ir distance at the terrace, amounting to θ_d = 0.21. At low energies (E_i < 0.1 eV), the dissociation of CH_4 on Ir(332) almost exclusively takes place in the step zone as the barrier at terrace sites is too high (Figure 3c). Interestingly, in addition to the direct reactive trajectories occurring at steps with a single bounce on the surface (corresponding to an impact time less than ~800 fs, see below), we find that a significant number of trajectories initially impacting on terraces, diffuse to the step zone and indirectly dissociate at steps before desorption. As pointed out by Moriaghi *et al*.[39] and shown in our earlier AIMD study,[35] these temporarily trapped molecules are not completely thermalized and highly mobile. This is supported by the distributions of impact time and traveling distance (d_{xy}) of $CH_4(1\nu_3)$ on parallel to the surface of reactive trajectories at E_i = 0.03 eV, as displayed in Figure 4. Interestingly, we find an apparent separation in the timeline of reactive trajectories from ~800 to ~1300 fs. This provides us a reasonable criterion to separate direct and indirect (or trapped) trajectories. Indirect reactive trajectories stick to the surface till the end of propagation (~10 ps) with a long travel distance (d_{xy}) on the surface up to 77 Å. This trapping-mediated mechanism appears different from the H_2+Pt case recently discussed by van Lent et al.,[13] in which these authors suggested the trapping-mediated mechanism takes place at the step cusp involving sufficient kinetic energy dissipation and no diffusion.

Although propagation until all trapped molecules undergo either desorption or reaction is numerically too expensive even with the aid of an analytical PES, the results already shed some valuable light on the dynamics of these precursors. In particular, the proportion of remaining physisorbed molecules on both the Ir(111) and Ir(332) surfaces decays exponentially, as shown in Figure 5, suggesting a simple first-order activated process. Such

a behavior offers supporting evidence for the statistical treatment advocated by Jackson,[40] even when the motion along thermalized with the surface. The slope of the decay curve in a log plot thus provides information on the trapping lifetimes for CH_4, which are estimated as 18.3 ± 0.6 and 12.0 ± 0.1 ps on Ir(111) and Ir(332) at E_i = 0.03 eV (see Figure 5), respectively. The calculated lifetime on Ir(111) is larger than earlier theoretical estimates, *e.g.*, ~13 ps[39] and ~8 ps[36] obtained in MD studies, and 6.5 ps deduced from the desorption rate.[40], Despite the deepest adsorption well among all the theoretical calculations, interestingly, the estimated lifetime (desorption rate) reported in Ref. 40 is smallest (fastest), due presumably to the approximate partition functions used in the transition-state theory calculation of the rate constant.

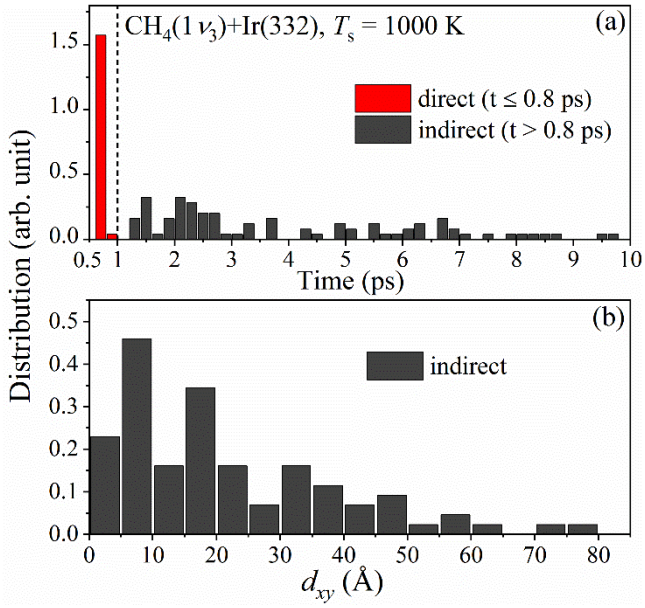

Figure 4. Distributions of (a) impact time and (b) accumulated moving distance of $CH_4(1\nu_3)$ parallel to the Ir(332) surface extracted from reactive trajectories at E_i = 0.03 eV, T_s = 1000 K.

An interesting observation from our dynamical calculations is that the vibrationally excited CH_4 behaves roughly the same as its unexcited counterpart in both low and high incident energies, except with higher reactivity. The higher reactivity is apparently due to the energy deposited in the asymmetric stretching mode of CH_4, which aligns with the reaction coordinate well. According to the Sudden Vector Projection model,[22, 54] this strong overlap allows a promotional effect on the reactivity because of facile energy flow into the reaction coordinate at the transition state. What is remarkable is the promotional effect remains for the trapped molecules, as observed experimentally,[33] and confirmed theoretically here and before.[39] This can be attributed to the extremely inefficient energy flow from the high-frequency vibrational mode to the low-frequency translational, rotational and surface phonon modes. In particular, the excitation of electron-hole pairs is expected to slightly reduce S_0 to some extent but not change the shape of S_0 curve as found previously[55, 56]. This is supported by an increasing body of experimental and theoretical evidence,[33, 39, 57, 58] suggesting vibrational mode specificity might still play an important role in precursor-mediated dissociation.

The aforementioned QCT results clearly suggest that a precursor-mediated reaction mechanism requires two necessary steps. First, the molecules have to be trapped for a sufficiently long time, and second, they need to find a defect site with a sufficiently low barrier to react. Importantly, we conclude based on results presented above that the precursor-mediated mechanism is facilitated by defect sites on the Ir(111) surface and assisted by thermal motion, rather than merely by the thermally induced temporary puckering of surface atoms on the perfect Ir(111) surface, as suggested by Busnengo and coworkers.[39] Interestingly, our results are consistent with the latest work of Jackson who also found that defects can contribute significantly to indirect methane dissociation on Ir surfaces.[40] Both Jackson and we used non-local functionals with dispersion correction, which are known to be more reliable than the semi-local PBE functional in describing the van der Waals well, which plays an important role in trapping and diffusion.

Figure 5. Trapping probabilities of CH_4 on (a, b) Ir(111) and (c, d) Ir(332) as a function of

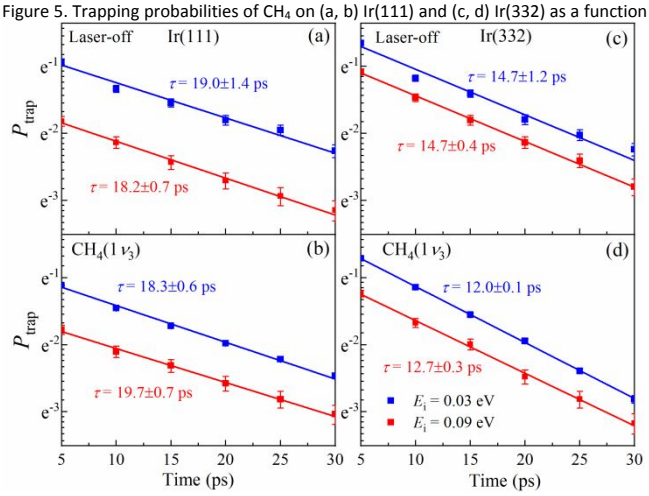

time in laser-off conditions (top panels) and the $(1\nu_3)$ state (bottom panels) at various incident energies with T_s = 1000 K.

The aforementioned conclusion motivates us to propose the model introduced in Sec. II. To validate this model, we take the Ir(332) surface as an example with a step density θ_d = 0.21 and L_d = 12.92 Å. All other necessary parameters in our model have been extracted from QCT calculations for CH_4 in laser-off and $(1\nu_3)$ conditions on Ir(111), respectively (see Table S6), as discussed in Sec. II. Specifically, the initial trapping probability P_{trap} is the fraction of trajectories with multiple bounces characterized by an impact time longer than ~800 fs. It is seen from Figure 5 that the lifetime of a molecule in the physisorption state is insensitive to the internal (vibrational) energy and translational energy in the low-E_i regime (E_i < 0.1 eV), so is the average lateral velocity of trapped molecules. We thus take an averaged τ of ~19 ps and an averaged v of ~6 Å/ps for trapped laser-off CH_4 and $CH_4(1\nu_3)$ molecules on the terrace at T_s = 1000 K. The results do not change qualitatively if somewhat different values are used.

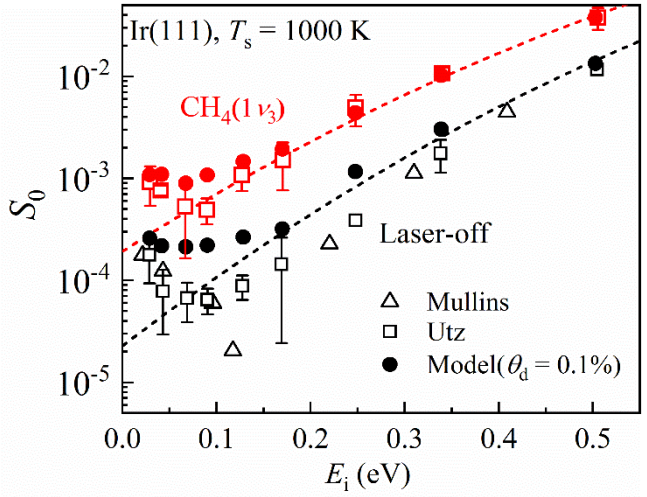

Figure 6. The same as Figure 2, except that the theoretical data are predicted by the proposed model taking 0.1% of defect density into account.

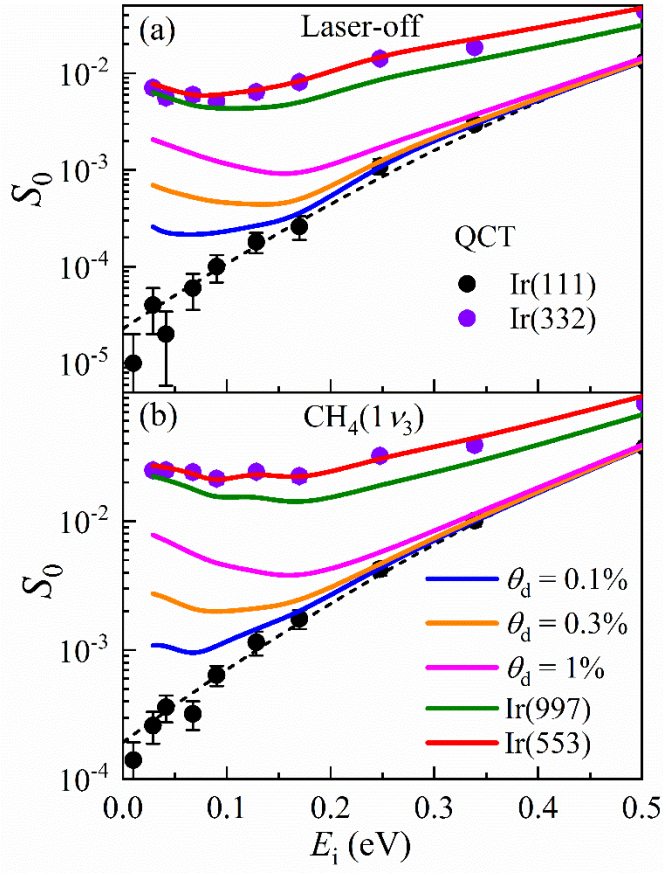

Figure 7. Predicted S_0 curves of CH_4 in (a) laser-off conditions and (b) ($1\nu_3$) state on Ir(111) with various defect densities (θ_d) at T_s = 1000 K by the proposed model. The QCT results on Ir(111) (black circles) and Ir(332) (violet circles) are shown for comparison.

The model successfully reproduces the QCT calculated S_0 curves in the entire energy range, including their negative dependence on E_i at low energies, as shown in Figure 3a. The good agreement between the model and QCT results allows us to analyze the contributions of direct and indirect components and the influence of step defects on CH_4 dissociative chemisorption. To this end, we demonstrate this point using the statistically more reliable results of $CH_4(1\nu_3)$, while the results in laser-off conditions display similar behaviors. Figure 3d clearly shows that the P_{trap} decreases exponentially as a function of E_i, resulting in the same E_i-dependence of the indirect sticking probability at steps ($S_{0,defect}^{indirect}$). As discussed by Moriaghi *et al.*[39] based on their more reactive RFF, $S_0^{indirect}$ and P_{trap} on Ir(111) have the same dependence on E_i but differ by a constant factor which is independent of E_i. We find a similar behavior here and P_{trap} for $CH_4(1\nu_3)$ is about 29 times of $S_{0,defect}^{indirect}$ on Ir(332). By contrast, the direct sticking probabilities at both step and terrace sites increase monotonically with E_i. The former are much higher than the latter at low energies but they become comparable at E_i = 0.5 eV. These results clearly demonstrate that the step sites dominate the dissociation of CH_4 on Ir(332) at low energies and the negative activation of S_0 on Ir(332) below 0.1 eV is mainly due to the significant indirect contribution from step sites in this energy regime.

Let us turn back to the imperfect Ir(111) and analyze the possible role of trace defects. Indeed, the density of defect sites on the cleaved Ir(111) surface used in the experiment was estimated to be at most 0.5%.[31] This seems rather small, but the reactivity on these sparse defect sites can be very important at low energies. Using the step reactivity information extracted from QCT calculations on Ir(332), we estimate the S_0 curve on imperfect Ir(111) by the model considering merely 0.1% of defects. Not surprisingly, the predicted S_0 curve significantly improves the agreement with experiments in the low E_i regime and explicitly shows a negative dependence with E_i in Figure 6. This result is consistent with Jackson's estimation from a more approximate model,[40] suggesting that even such a tiny fraction of defects can make a significant contribution to the low energy reactivity and may also be possible source of the experimentally observed precursor-mediated mechanism. Our model appears to overestimate to some extent the indirect sticking probabilities between E_i = 0.05~0.15 eV in laser-off condition, due presumably to the assumption of total energy scaling of $S_{0,defect}^{direct}$ to estimate P_{diss}. A detailed comparison of defect contributions between our and Jackson's models is presented in Figure S6 of the SI. Both models give the same trend, but our model leads to a much larger $S_{0,defect}^{indirect}$. This may be improved by a more precise determination of P_{diss} at a given v, which deserves further investigations. We note in passing that obtaining T_s-dependent S_0 data in our model is more expensive than the transition state theory based model of Jackson,[40] as P_{diss} will depend strongly on T_s and has to be simulated separately in our model. We will defer the study of the temperature effect to future work.

Finally, with this simple model, we are in a position to predict S_0 curves of CH_4 on Ir surfaces with different θ_d, without resorting to expensive dynamical calculations in each case. Figure 7 shows that the low-energy reactivity increases drastically with the small amount of increase of the step density, *e.g.*, from 0.1% to 1%. While once the step density gets larger, the S_0 values increase more mildly, *e.g.* for Ir(997) and Ir(553), which have the same type of step sites as (332). In any cases, the indirect channel appears to be dominant at low energies. This has significant implications to methane steam reforming in realistic conditions, under which the defect-induced precursor-mediated dissociation of methane on practical catalysts may play a more important role than

imagined before. These predictions present testable scenarios for experimental verification of the current model.

Conclusions

In this work, we report extensive quasi-classical dynamics of methane dissociation on two different Ir surfaces in a wide range of incidence energies, aimed at a more in-depth understanding of the reaction mechanism and influence of defect sites on the reactivity. These dynamic calculations were performed on a unified high-dimensional PES, which is determined from DFT data by machine learning for not only the methane interacting with the (322) facet of Ir, in which the step sites can be regarded as a proxy for defects, but also the (111) terrace. It is shown that the dissociation is exclusively direct at high incidence energies, but a large fraction of impinging molecules become trapped at low incidence energies, undergoing extensive diffusion on the surface. For these molecules, reaction mediated by these trapped precursors competes with desorption, both requiring long time dynamics. Such long time dynamics are not amenable to direct dynamics simulations, but viable with an analytic PES. Our results strongly suggest that the experimentally observed "negatively activated" regime for the dissociation of both the ground and vibrationally excited methane on hot Ir(111) at low incidence energies does not stem from dissociation on terrace sites, because the temperature effect is found to be insufficient for the trapped CH_4 to react. Instead, a combination of a lower dissociation barrier at the step site and surface atom fluctuation at high surface temperatures is shown to be responsible for the experimental observation.

These trajectories also provide valuable information on the direct reaction, trapping, and indirect reaction channels; and allow us to propose a first-principles-based dynamic model to describe the overall dissociative chemisorption of CH_4 on flat Ir surfaces, including those decorated with defects. In this model, direct sticking on both terraces and steps is explicitly simulated using an accurate potential energy surface, while indirect dissociation at defect sites is modeled by the first-principles-determined lifetime of the physisorbed molecule on the terrace and its non-equilibrium diffusing velocity, as well as the estimated step-step distance. We demonstrate that this model is able to capture the experimentally observed S_0 curve on Ir(111) at very low energies with a step-density of 0.1~0.5%, as well as the S_0 curve calculated on the stepped Ir(332) surface. This approach thus allows us to provide an adequate description for defect-sensitive reactivity of a variety of surface reactions with a varying step density for both the ground and vibrationally excited methane. These detailed calculations and insights help to bridge the structure gap in heterogeneous catalysis.

Conflicts of interest

Authors declare no conflict of interests.

Acknowledgements

B. J. was supported by National Key R&D Program of China (2017YFA0303500), National Natural Science Foundation of China (91645202, 21722306), and Anhui Initiative in Quantum Information Technologies (AHY090200). H. G. thanks the Alexander von Humboldt Foundation of a Humboldt Research Award and National Science Foundation for generous support (CHE-1462109 and CHE-1951328). We thank the Supercomputing Center of University of Science and Technology of China and the Center for Advanced Research Computing at University of New Mexico for high-performance computing services.

References

1. T. Zambelli, J. Wintterlin, J. Trost and G. Ertl, *Science*, 1996, **273**, 1688-1690.
2. S. Dahl, A. Logadottir, R. C. Egeberg, J. H. Larsen, I. Chorkendorff, E. Tornqvist and J. K. Nørskov, *Phys. Rev. Lett.*, 1999, **83**, 1814-1817.
3. K. Honkala, A. Hellman, I. N. Remediakis, A. Logadottir, A. Carlsson, S. Dahl, C. H. Christensen and J. K. Nørskov, *Science*, 2005, **307**, 555-558.
4. S. L. Bernasek, W. J. Siekhaus and G. A. Somorjai, *Phys. Rev. Lett.*, 1973, **30**, 1202-1204.
5. D. A. McCormack, R. A. Olsen and E. J. Baerends, *J. Chem. Phys.*, 2005, **122**, 194708.
6. I. M. N. Groot, A. W. Kleyn and L. B. F. Juurlink, *Angew. Chem. Int. Ed.*, 2011, **123**, 5280-5283.
7. D. Migliorini, H. Chadwick, F. Nattino, A. Gutiérrez-González, E. Dombrowski, E. A. High, H. Guo, A. L. Utz, B. Jackson, R. D. Beck and G.-J. Kroes, *J. Phys. Chem. Lett.*, 2017, **8**, 4177-4182.
8. G. Füchsel, K. Cao, S. Er, E. W. F. Smeets, A. W. Kleyn, L. B. F. Juurlink and G.-J. Kroes, *J. Phys. Chem. Lett.*, 2018, **9**, 170-175.
9. H. Chadwick, H. Guo, A. Gutiérrez-González, J. P. Menzel, B. Jackson and R. D. Beck, *J. Chem. Phys.*, 2018, **148**, 014701.
10. H. Chadwick, A. Gutiérrez-González, R. D. Beck and G.-J. Kroes, *J. Phys. Chem. C*, 2019, **123**, 14530-14539.
11. H. Guo and B. Jackson, *J. Chem. Phys.*, 2019, **150**, 204703.
12. K. Cao, R. van Lent, A. W. Kleyn, M. Kurahashi and L. B. F. Juurlink, *Proc. Natl. Acad. Sci. U. S. A.*, 2019, DOI: 10.1073/pnas.1902846116, 201902846.
13. R. van Lent, S. V. Auras, K. Cao, A. J. Walsh, M. A. Gleeson and L. B. F. Juurlink, *Science*, 2019, **363**, 155-157.
14. J. Neugebohren, D. Borodin, H. W. Hahn, J. Altschäffel, A. Kandratsenka, D. J. Auerbach, C. T. Campbell, D. Schwarzer, D. J. Harding, A. M. Wodtke and T. N. Kitsopoulos, *Nature*, 2018, **558**, 280-283.
15. L. Vattuone, L. Savio and M. Rocca, *Surf. Sci. Rep.*, 2008, **63**, 101-168.
16. B. Poelsema, K. Lenz and G. Comsa, *J. Phys.: Condens. Matter*, 2010, **22**, 304006.
17. B. Poelsema, K. Lenz and G. Comsa, *J. Chem. Phys.*, 2011, **134**, 074703.
18. L. Zhou, A. Kandratsenka, C. T. Campbell, A. M. Wodtke and H. Guo, *Angew. Chem. Int. Ed.*, 2019, **58**, 6916-6920.
19. L. B. F. Juurlink, D. R. Killelea and A. L. Utz, *Prog. Surf. Sci.*,

2009, **84**, 69-134.
20. H. Chadwick and R. D. Beck, *Annu. Rev. Phys. Chem.*, 2017, **68**, 39-61.
21. A. K. Tiwari, S. Nave and B. Jackson, *Phys. Rev. Lett.*, 2009, **103**, 253201.
22. B. Jiang, R. Liu, J. Li, D. Xie, M. Yang and H. Guo, *Chem. Sci.* , 2013, **4**, 3249-3254.
23. X. J. Shen, A. Lozano, W. Dong, H. F. Busnengo and X. H. Yan, *Phys. Rev. Lett.*, 2014, **112**, 046101.
24. F. Nattino, H. Ueta, H. Chadwick, M. E. van Reijzen, R. D. Beck, B. Jackson, M. C. van Hemert and G.-J. Kroes, *J. Phys. Chem. Lett.*, 2014, **5**, 1294-1299.
25. S. Nave, A. K. Tiwari and B. Jackson, *J. Phys. Chem. A*, 2014, **118**, 9615-9631.
26. H. Guo, A. Farjamnia and B. Jackson, *J. Phys. Chem. Lett.*, 2016, **7**, 4576-4584.
27. B. Jiang, M. Yang, D. Xie and H. Guo, *Chem. Soc. Rev.*, 2016, **45**, 3621-3640.
28. X. Shen, Z. Zhang and D. H. Zhang, *J. Chem. Phys.*, 2017, **147**, 024702.
29. B. Jiang and H. Guo, *J. Chem. Phys.*, 2019, **150**, 180901.
30. D. C. Seets, M. C. Wheeler and C. B. Mullins, *J. Chem. Phys.*, 1997, **107**, 3986-3998.
31. D. C. Seets, C. T. Reeves, B. A. Ferguson, M. C. Wheeler and C. B. Mullins, *J. Chem. Phys*, 1997, **107**, 10229-10241.
32. T. A. Jachimowski, C. J. Hagedorn and W. H. Weinberg, *Surf. Sci.*, 1997, **393**, 126-134.
33. E. Dombrowski, E. Peterson, D. Del Sesto and A. L. Utz, *Catal. Today*, 2015, **244**, 10-18.
34. A. V. Walker and D. A. King, *Phys. Rev. Lett.*, 1999, **82**, 5156-5559.
35. R. Bisson, M. Sacchi and R. D. Beck, *J. Chem. Phys*, 2010, **132**, 094702.
36. G. O. Sitz and C. B. Mullins, *J. Phys. Chem. B*, 2002, **106**, 8349-8353.
37. G. Henkelman and H. Jònsson, *Phys. Rev. Lett.*, 2001, **86**, 664-667.
38. R. Moiraghi, A. Lozano and H. F. Busnengo, *J. Phys. Chem. C*, 2016, **120**, 3946-3954.
39. R. Moiraghi, A. Lozano, E. Peterson, A. Utz, W. Dong and H. F. Busnengo, *J. Phys. Chem. Lett.*, 2020, **11**, 2211-2218.
40. B. Jackson, *J. Chem. Phys.*, 2020, **153**, 034704.
41. X. Zhou, B. Jiang and H. Guo, *J. Phys. Chem. C*, 2019, **123**, 20893-20902.
42. G. Kresse and J. Furthmuller, *Phys. Rev. B*, 1996, **54**, 11169-11186.
43. G. Kresse and J. Furthmuller, *Comp. Mater. Sci.*, 1996, **6**, 15-50.
44. J. Klimeš, D. R. Bowler and A. Michaelides, *J. Phys.: Condens. Matter*, 2010, **22**, 022201.
45. Y. Zhang, C. Hu and B. Jiang, *J. Phys. Chem. Lett.*, 2019, **10**, 4962-4967.
46. Y. Zhang, C. Hu and B. Jiang, *Phys. Chem. Chem. Phys.*, 2020, DOI: 10.1039/D0CP05089J.
47. B. Jiang, J. Li and H. Guo, *J. Phys. Chem. Lett.*, 2020, **11**, 5120-5131.
48. I. M. N. Groot, A. W. Kleyn and L. B. F. Juurlink, *J. Phys. Chem. C*, 2013, **117**, 9266-9274.
49. A. Al Taleb, G. Anemone, L. Zhou, H. Guo and D. Farías, *J. Phys. Chem. Lett.*, 2019, **10**, 1574-1580.
50. J. P. Perdew, K. Burke and M. Ernzerhof, *Phys. Rev. Lett.*, 1996, **77**, 3865-3868.
51. F. Nattino, D. Migliorini, G.-J. Kroes, E. Dombrowski, E. A. High, D. R. Killelea and A. L. Utz, *J. Phys. Chem. Lett.*, 2016, **7**, 2402-2406.
52. A. L. Walter, F. Schiller, M. Corso, L. R. Merte, F. Bertram, J. Lobo-Checa, M. Shipilin, J. Gustafson, E. Lundgren, A. X. Bríon-Ríos, P. Cabrera-Sanfelix, D. Sánchez-Portal and J. E. Ortega, *Nat. Commun.*, 2015, **6**.
53. A. J. Walsh, R. v. Lent, S. V. Auras, M. A. Gleeson, O. T. Berg and L. B. F. Juurlink, *J. Vac. Sci. Technol. A*, 2017, **35**, 03E102.
54. H. Guo and B. Jiang, *Acc. Chem. Res.*, 2014, **47**, 3679-3685.
55. B. Jiang, M. Alducin and H. Guo, *J. Phys. Chem. Lett.*, 2016, **7**, 327-331.
56. X. Luo, B. Jiang, J. I. Juaristi, M. Alducin and H. Guo, *J. Chem. Phys.*, 2016, **145**, 044704.
57. P. R. Shirhatti, I. Rahinov, K. Golibrzuch, J. Werdecker, J. Geweke, J. Altschäffel, S. Kumar, D. J. Auerbach, C. Bartels and A. M. Wodtke, *Nat. Chem.*, 2018, **10**, 592-598.
58. M. Huang, X. Zhou, Y. Zhang, L. Zhou, M. Alducin, B. Jiang and H. Guo, *Phys. Rev. B*, 2019, **100** 201407(R).